Crack patterns identification in masonry structures with a C° displacement energy method

Antonino Iannuzzo, Fabiana De Serio, Antonio Gesualdo and Giulio Zuccaro

Department of Structures for Engineering and Architecture,
University of Naples Federico II,
via Claudio 21,
Napoli 80125, Italy
Email: gesualdo@unina.it
Email: fabiana.deserio@gmail.com
Email: antonino.iannuzzo@unina.it
Email: zuccaro@unina.it

Antonio Fortunato and Maurizio Angelillo*

Department of Civil Engineering,
University of Salerno,
via Giovanni Paolo II 132,
Fisciano (SA) 84084, Italy
Email: mangelillo@unisa.it
Email: a.fortunato@unisa.it
*Corresponding author

Abstract: This paper deals with the analysis of fracture identification of a generic masonry structure subjected to loads and to kinematical actions (settlements, distorsions). The masonry is composed of normal rigid no-tension material (NRNT), that is a Heyman's material treated as a continuous body. An energy minimum criterion is used to solve the equilibrium problem, using continuous (C°) displacement fields and adopting a classical Finite Element approximation for the geometrical description. Some examples illustrate the way in which our approximate method detects crack patterns in some simple cases. The C° method, though more cumbersome form the numerical point of view, exhibits great efficiency in the identification of the exact location and orientation of the crack system, compared to methods based on discontinuous displacement fields.

Keywords: masonry; no-tension material; settlements and distorsions; C° displacement field; smeared cracks.

Reference to this paper should be made as follows: Iannuzzo, A., De Serio, F., Gesualdo, A., Zuccaro, G., Fortunato, A. and Angelillo, M. (2018) 'Crack patterns identification in masonry structures with a C° displacement energy method', *Int. J. Masonry Research and Innovation*, Vol. 3, No. 3, pp.295–323.

Biographical notes: Antonino Iannuzzo have gained his PhD in Structural Engineering, Geotechnical and Seismic at the University of Naples Federico II. His research areas, besides the modelling of masonry structures and rocking of rigid blocks, include homogenisation of discrete structures and seismic vulnerability.

Fabiana De Serio, PhD in Structural Engineering, Geotechnical and Seismic at the University of Naples Federico II, carries out her research in the fields of No-Tension materials and in 3-d modelling of masonry structures.

Antonio Gesualdo is Assistant Professor of Structural Engineering at the University of Naples Federico II where he received his PhD in Structural Engineering. His research fields are limit analysis, masonry mechanics and homogenisation.

Giulio Zuccaro is an Associate Professor of Structural Engineering at the University of Naples Federico II. He is Scientific Director of several European Research Projects and is member of the Task Group 3 "Seismic Risk and Seismic Scenarios". He is the Director of the Plinius research center at LUPT, Napoli. His main research activities concern masonry mechanics and seismic vulnerability of structures.

Antonio Fortunato obtained a PhD in Structural Engineering at the University of Naples and thereafter in the University of Salerno, he has been a Postdoctoral Researcher fellow. His research interests cover a wide range of topics such as structural masonry analysis, fracture mechanics, variational optimisation problems with no-convex energies and biomechanics of running.

Maurizio Angelillo, is Professor of Structural Mechanics at the University of Salerno. He is the author of more than 100 scientific papers, several of which are published in leading international journals of Structural and Solid Mechanics. Masonry structures and unilateral materials behaviour, propagation of brittle fracture in elastic solids, brain and corneal biomechanics are his main research topics.

1 Introduction

The present work deals with the assessment of the crack pattern due to given kinematical data (settlements/distortions) in masonry-like structures. On adopting the Heyman's model (see Heyman, 1966), we extend it to masonry structures considered as continuous bodies on considering the material as normal rigid no tension (NRNT). This material allows for the application of the theorems of Limit Analysis (i.e., the safe and the kinematic theorem), as first suggested by Kooharian (1952). For the application of these Theorems to unilateral materials we refer to the works of Livesley (1978), Como (1992), Angelillo (2014, 2015), Brandonisio et al. (2013, 2015), Gesualdo et al. (2017), Angelillo et al. (2014), Fortunato et al. (2015, 2018).

A minimum energy criterion, based on a displacement approach, enables to study the solutions of some typical mixed boundary value problems (BVP) of structures made of NRNT material.

The energy for brittle materials consists of the potential energy of the applied loads, of the elastic and of the interface ones, this latter being the energy necessary to activate a cracks on internal surfaces (Gesualdo et al., 2014, 2017; Monaco et al., 2014; Angelillo et al., 2012, 2015, 2016; Gesualdo and Monaco, 2015). For Heyman's materials, the energy is given only by the potential energy of the loads (De Serio et al., 2017). In the case of combined loads a wide range of bounding conditions are suggested in Fraldi et al. (2009); as a support to the monitoring of existing structures the method is also very useful (see Cennamo et al., 2013), as well as in the thrust network analysis (Marmo et al., 2018; Marmo and Rosati, 2017), or for time histories analyses in earthquakes as in Cennamo et al. (2017) and in the analysis of collapse risk of masonry structures in the cities (Cennamo et al., 2017; Calderoni et al., 2016).

In order to search for the minimal solution of the energy a C° displacement method is proposed and discussed, approximating the solution in the set of continuous (C°) displacements. It is worth pointing out that, though for NRNT materials singular (i.e., concentrated) strains are admitted, with the C° method the strain exhibits only a regular part.

With the C° method, the minimum search can be undertaken approximately by using classical finite element (FE) approximations for the geometrical description of the problem. For unilateral material, a similar C° based displacement procedure has been already introduced in the paper by Angelillo et al. (2010) for the parent case of normal elastic no-tension (NENT) materials. What can be seen from Angelillo et al. (2010) by looking at some benchmark examples, is that, when the exact solution presents strain concentrations on some internal lines (cracks), the numerical solution exhibits large gradients (tending to become infinite for finer mesh sizes), on narrow bands approximating the fracture lines. The C° solution appears as more adaptable than the rigid block approximation (e.g., the piecewise rigid displacement (PR) method), as exposed in Iannuzzo et al. (2018), in approximating fracture lines that are far from being located along the skeleton of the mesh.

Some benchmark problems are examined to explain the ability of the C° method to predict crack patterns and the correspondent piecewise rigid displacement field as well as the partition into rigid blocks in which the structures separate during their movements. Finally, the last application involves a masonry portal undergoing some experimental tests (see Augenti et al., 2010) and exhibiting typical fracture patterns in the spandrel. As a result of a comparison of real fracture pattern with those predicted by our model, it is seen that the predictions of the proposed model are in good agreement with the laboratory outcomes.

2 NRNT materials and BV problem

NRNT materials. The Heyman's model can be extended to two-dimensional continua imposing unilateral material restrictions on the stress and suitable assumptions on the latent strain i.e., on the inelastic deformation associated to bear the stress unilateral constraint. A 2d masonry structure S, is modelled as a continuum Ω of the Euclidean space $\mathcal{E}^2$. The stress inside Ω is denoted by T and the displacement of material points x

belonging to Ω with the symbol *u*. The linear strain *E* is adopted as the strain measure, restricting to of small displacements and strains.

The NRNT material is characterised by the following restrictions:

$$T \in Sym^{-},\ E \in Sym^{+},\ T \cdot E = 0\ , \tag{1}$$

being Sym^{-} ,Sym^{+} the mutually polar cones of negative semidefinite and positive semidefinite symmetric tensors. Restrictions (1) are equivalent to the following normality conditions:

$$T \in Sym^{-}\ ,\ \left(T - T^{*}\right) \cdot E \geq 0\ ,\ \forall T^{*} \in Sym^{-} \tag{2}$$

and, dually, to the so called *dual normality conditions*:

$$E \in Sym^{+},\ \left(E - E^{*}\right) \cdot T \geq 0,\ \forall E^{*} \in Sym^{+}. \tag{3}$$

The restrictions (2) defining the NRNT material are the principal elements for the application of the Limit Analysis theorems (see Kooharian, 1952; Giaquinta and Giusti, 1985; Livesley, 1978; Fortunato et al., 2014, 2016).

The BV problem. The equilibrium of a 2d masonry structure, modelled as a continuum made of NRNT material and subject to loads and settlements, can be expressed as a Boundary Value Problem (BVP) as follows: *"Find a displacement field u and the allied strain E, and a stress field T such that*

$$E = \frac{1}{2}\left(\nabla u + \nabla u^{T}\right),\ E \in Sym^{+},\ u = \overline{u}\ \text{on}\ \partial\Omega_{D} \tag{4}$$

$$divT + b = 0\ \ ,\ \ T \in Sym^{-}\ \ ,\ \ Tn = \overline{s}\ \text{on}\ \partial\Omega_{N} \tag{5}$$

$$T \cdot E = 0 \tag{6}$$

where **n** is the unit outward normal to the boundary δΩ, and $\delta\Omega_D$, $\delta\Omega_N$ is a fixed partition of the boundary into constrained and loaded parts respectively (Angelillo and Fortunato, 2004).

An important role is played by the set *K* of kinematically admissible displacements, and the set *H* of statically admissible stresses, defined by:

$$K = \left\{ u \in S\ \ /\ E = \frac{1}{2}\left(\nabla u + \nabla u^{T}\right) \in Sym^{+}\ \ \&\ \ u = \overline{u}\ \ \text{on}\ \partial\Omega_{D} \right\}, \tag{7}$$

$$H = \left\{ T \in S^{'}\ /divT + b = 0\ ,\ T \in Sym^{-},\ \ \ Tm = \overline{s}\ \text{on}\ \partial\Omega_{N} \right\} \tag{8}$$

with $S.S'$ two suitable function spaces.

A solution of the BVP for masonry-like structures is a triplet $\left(u^{\circ}, E\left(u^{\circ}\right), T^{\circ}\right)$ such that: $u^{\circ} \in K$, $T^{\circ} \in H$, and $T^{\circ} \cdot E\left(u^{\circ}\right) = 0.$

3 The kinematical problem (KP): an energy approach

The adoption of a displacement approach to a structure subject to given loads and distortions, consists in the search of a displacement field $u \in K$ for which there exist a stress field $T \in H$ such that $T \cdot E(u) = 0$. In order to solve the BVP with a displacement method, a criterion based on the minimisation of an energy function $\wp(u)$ depending on *u* is considered.

The minimiser of $\wp(u)$ over the set *K*, is the solution of the BVP under the restrictions (1), then it ensures the equilibrium of the loads applied on the structure.

For NRNT materials, the total potential energy reduces to the potential energy of the loads, that is to a linear functional of *u*. The minimum energy problem can be formulated as follows: "*Find a displacement field* $u^\circ \in K$ *, such that*

$$\wp(u^\circ) = \min_{u \in K} \wp(u) \ , \tag{9}$$

where

$$\wp(u) = -\int_{\partial\Omega_N} \overline{s} \cdot u \, \mathrm{d}s - \int_\Omega b \cdot u \, \mathrm{d}a, \tag{10}$$

is the potential energy of the given loads and K is the set of kinematically admissible displacements, defined in equation (7).

The proof of the existence of the minimiser u° of $\wp(u)$ for $u \in K$, is a complex mathematical question and is beyond the scopes of the present paper. The interested reader can refer to the papers (Giaquinta and Giusti, 1985; Anzellotti, 1985), where the existence of the minimum is discussed, with the direct method of the calculus of variation, for the parent problem concerning elastic normal no-tension materials. In those papers the existence of the minimiser u° of the total potential energy for $u \in BD(\Omega)$, is proved under some restrictions on the given loads (among which the main assumption is the so-called *safe load condition*: see *Remark 4*), in the case either of pure traction problems or pure displacements problems: the case of mixed problem is not covered. On assuming that the *KP* is compatible (i.e., $K \neq \varnothing$), what we can easily show is that:

- If the load is compatible (i.e., $H \neq \varnothing$) the linear functional $\wp(u)$ is bounded from below.
- If the triplet $(u^\circ, E(u^\circ), T^\circ)$ is a solution of the BVP, it corresponds to a weak minimum of the functional $\wp(u)$.

These simple proofs of the propositions a and b are reported in Iannuzzo et al. (2018).

4 The C° method: theory and numerical implementation

4.1 C° method: theory

The minimisation strategy based on continuous (C^0) displacement fields reduces to a classical approximation procedure based on a FE mesh, for which the strain is purely regular: the approximation of the minimum problem (17) through C^0 functions yields to a

classical FEM-like formulation, whilst the use of piecewise rigid displacements (as in Iannuzzo et al., 2018) can be thought of as belonging to the class of so-called discrete element methods (see Sarhosis et al., 2016), and for application (Simon and Bagi, 2016)).

The formulation of the C^0 method proceeds as follows. The first simplification consists in considering only the infinite dimensional subset of K constituted by continuous functions. The second approximation is to restrict to a finite subset of it, by discretising the domain Ω into a number M of elements with the finite partition

$$(\Omega_i)_{i\in\{1,2,..,M\}}, \tag{11}$$

such that

$$\sum_{i=1}^{M} P(\Omega_i) < \infty, \tag{12}$$

$P(\Omega_i)$ being the perimeter of Ω_i. In particular, in what follows, we refer to polygonal elements, such that the boundary $\partial\Omega_i$ of the n-polygon Ω_i, is composed of n segments Γ linking n points.

Remark 3: We remark that, whilst with the PR method (see Iannuzzo et al., 2018), the interfaces between blocks play a crucial role, being potential fracture lines, with the second method two nodes belonging to two different elements must have the same displacements, and then the interfaces play a secondary role. ■

Assuming the continuity of the displacement field at the nodes, the NRT material restrictions have to be enforced on the strain arising inside the elements. In particular, recalling definition (1), the normal rigid no-tension material (NRNT) is completely defined by the restrictions:

$$T \in Sym^{-},\ E \in Sym^{+},\ T \cdot E = 0\ . \tag{13}$$

On approaching the problem as an energy minimisation of the type (9), that is with a displacement approach, the latent strain E has to belong to the positive semidefinite cone:

$$E \in Sym^{+}. \tag{14}$$

This restriction, for 2d problems, is equivalent to the two following inequalities:

$$trE \geq 0,\ detE \geq 0\ . \tag{15}$$

In the 2d Euclidean space, a generic tensor, such as the latent strain E can be represented, in a fixed Cartesian reference, by a 2x2 matrix:

$$E = \begin{bmatrix} \varepsilon_{11} & \varepsilon_{12} \\ \varepsilon_{21} & \varepsilon_{22} \end{bmatrix}. \tag{16}$$

Geometrically, the condition $detE \geq 0$ defines a double cone in the space Sym, and the additional condition $trE \geq 0$ selects one of the two parts of the cone, namely the set of semidefinite positive symmetric tensors which is a convex cone. In particular, analytically, such restrictions can be conveniently represented in graphical form with reference to the three dimensional space Sym spanned by the dyadic orthonormal base

$(e_1 \otimes e_1 , e_2 \otimes e_2 , \sqrt{2}(e_1 \otimes e_2 + e_2 \otimes e_1))$, conditions (15) can be written in terms of Cartesian components, as:

$$\varepsilon_{11}\varepsilon_{22} - \varepsilon_{12}{}^2 \geq 0 \ , \ \ \varepsilon_{11} + \varepsilon_{22} \geq 0 \ , \tag{17}$$

which can easily be expressed as conditions on the displacement field u since $E = Sym\nabla u$. We choose to implement numerically conditions (17) in an approximate way in order to preserve the linearity of the problem. The typical way to do so is to approximate the cone Sym^+ through a plane envelope. The linearisation of conditions (17) is described in detail in Section 6.2 (item 4).

The partition $(\Omega_i)_{i\in\{1,2,..,M\}}$ constitutes a discretisation of the geometrical domain, the displacement field u is a function of the nodal displacements, as sketched in Figure 1. In particular, let $\hat{U} \in R^{2N}$ be the vector which collects the displacement components of the $2N$ nodes, the displacement field can be expressed as a functions of the node displacements:

$$u = u(\hat{U}) \ , \tag{18}$$

where $\hat{U} = (U_1, V_1, .., U_i, V_i, .., U_N, V_N)$ and (U_i, V_i) denotes the displacement of the node i. If K_c^N denotes the finite subspace of SBV defined by the continuous functions associated with the finite element chosen, the minimum problem can be written as follows:

$$\wp(\hat{u}) = \min_{u\in K_c^N} \wp(u) \ , \tag{19}$$

in which the continuous displacement $u \in K_c^N$ is expressed by $2N$ scalar parameters, that are the components of the displacements of the N nodes of the given mesh.

Figure 1 The infinite dimensional space K_c of continuous displacements with support in Ω: (a) is discretised considering a partition $(\Omega_i)_{i\in\{1,2,..,M\}}$ of the whole domain into e.g., quadrangular elements; (b) the finite dimensional approximation generated by the fixed partition is called K_c^N, where N is the number of nodes. In (c) a subdomain Ω_k and a second order Lagrangian element with 9 nodes is depicted

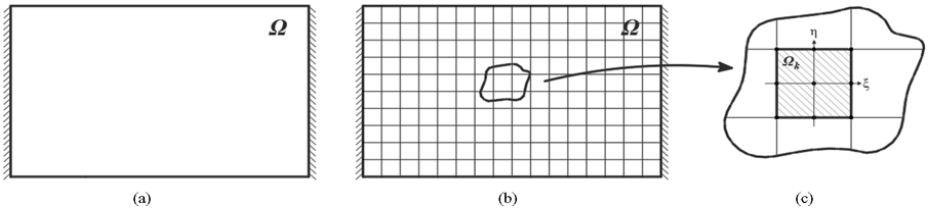

These parameters are restricted by the assumption that the strain must belong to the cone Sym^+. We recall that the condition $E \in Sym^+$ is enforced in an approximated way by restricting E to belong to an envelope of a finite number of tangent plane. Therefore the

only internal restrictions that we have in this case are linear inequalities, which can be expressed in terms of the unknown nodal displacements. In matrix form:

$$A\hat{U} \geq 0. \tag{20}$$

Finally, with the proposed FE approximations, the minimum problem (19) which approximates the minimum problem (9) can be transformed into

$$\wp\left(\hat{U}^0\right) = \min_{\hat{U} \in K^N} \wp\left(\hat{U}\right) \ , \tag{21}$$

K^N being the set

$$K^N = \{\hat{U} \in R^{2N} \ / A\ \hat{U} \geq 0\} \ . \tag{22}$$

4.2 C° method: numerical implementation

The solution of the specific problems here analysed is obtained by implementing the method with the program Mathematica ® (Wolfram, 2003). The implementation of the method proceeds into the following steps:

- definition of the structural geometry and of its discretisation
- discretisation of the displacement field over the given mesh
- explication of the potential energy in terms of the nodal displacement parameters
- explication of the side conditions
- numerical solution of the minimum problem with a linear programming routine
- post-processing (evaluation of displacement and strain corresponding to the approximate minimum solution).
- Let us denote Ω_* the domain of E^2 representing the structural geometry; consider the minimum rectangular domain Ω^* containing Ω_*. The whole domain Ω^* is partitioned into *N* rectangular basic units Ω_i, we call them subdomains. The set $\pi^* = \left(\Omega_i\right)_{i \in \{1,\ldots,N\}}$ constitutes a partition of Ω^*, that is:

$$\bigcup_{i=1}^{N} \Omega_i = \Omega^* \ \ \& \ \Omega_i \cap \Omega_j = \varnothing, \ \ \forall i, j \in \{1, \ldots, N\} \ / \ i \neq j \ . \tag{23}$$

To take into account the presence of voids (that is of subdomains of Ω^* not belonging entirely to in the domain Ω_*) it is necessary to perform an appropriate elimination of some elements belonging to π^*. To this purpose, we consider the set

$$\pi_M = \left\{\Omega_i \in \pi^* \ / \Omega_i \cap \Omega_* \neq \varnothing\right\} , \tag{24}$$

where *M* is the cardinality of π_M. Defining $\Omega = \bigcup_{\Omega_j \in \pi_M} \Omega_j$ from equation (38) it follows:

$$\Omega \supseteq \Omega_*. \tag{25}$$

Therefore π_M is a particular cover of the real structural domain Ω_*: it is the minimum cover of Ω_* (with respect to the cardinality) and at the same time it constitutes a finite partition of Ω, which becomes *our structural model domain*. Finally, it is to be noticed that π_M is a countable set of subdomains having finite perimeter, therefore, is a Caccioppoli partition of Ω in the sense of Chambolle et al. (2007).

- The displacement field $u = u(x)$, defined in Ω, is approximated through functions belonging to a subset of C^0 associated to the chosen cover π_M introduced in 1. The optimal choice, balancing accuracy and simplicity, turned out to be a second order Lagrangian quadrangular element. In what follows, we refer to this special kind of element and to its shape functions (Bathe and Wilson, 1976).

With reference to Figure 2, in the plane (ξ,η) the shape function $N_{ij} = N_{ij}(\xi,\eta)$ with $(i,j) \in \{1,2,3\}\times\{1,2,3\}$ is such that the maximum one-dimensional polynomial degree is of the second order (i.e., $\propto \xi^2, \eta^2$) whilst the maximum polynomial term is of the fourth order (i.e., $\propto \xi^2\eta^2$). In particular, denoting (ξ_i,η_j) the coordinates of the nodes: $N_{ij}(\xi_i,\eta_j) = 1$ and $N_{ij}(\xi_k,\eta_l) = 0$ for all $(k,l) \in \{1,2,3\}\times\{1,2,3\} \setminus (i,j)$.

Figure 2 Generic subdomain Ω_k : a second order Lagrangian element with 9 nodes

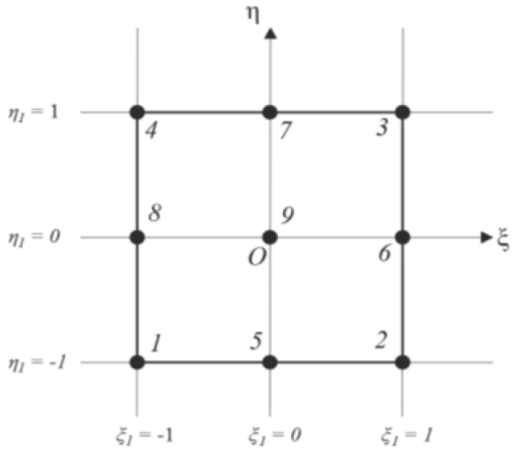

For example, the generic shape function could be obtained as the product of two one-dimensional second order Lagrangian shape functions, e.g., the shape function N_{23} is:

$$N_{23} = \frac{(\xi-\xi_1)(\xi-\xi_3)}{(\xi_2-\xi_1)(\xi_2-\xi_3)}\frac{(\eta-\eta_1)(\eta-\eta_2)}{(\eta_3-\eta_1)(\eta_3-\eta_2)} \tag{26}$$

Using the diffeomorphism *f*, namely:

$$f : (x,y) \in \Omega_k \to \big(\xi(x,y),\eta(x,y)\big), \tag{27}$$

it is possible to generate the shape functions for generic rectangles or quadrangles, associating to each node belonging to the domain Ω_k in the plane (x,y) the relative shape function $N_{ij}^f(x,y)$ defined as:

$$N_{ij}^f : (x,y) \in \Omega_k \to N_{ij} \circ f(x,y) . \tag{28}$$

In the global reference (O,x,y), denoting $l \in \{1,..,9\}$ the generic node of the finite element Ω_k, the displacement u_k can be expressed as:

$$u_k : (x,y) \in \Omega_k \to \sum_{l=1}^{9} N_l^f(x,y)(U_l,V_l) , \tag{29}$$

where (U_l,V_l) is the vector collecting the two unknown components of the translations of the nodes l. The global displacement is written as:

$$u : x \in \Omega \to \begin{cases} u_1, & \text{if } x \in \Omega_1 , \\ & \vdots \\ u_j, & \text{if } x \in \Omega_j , \\ & \vdots \\ u_M, & \text{if } x \in \Omega_M , \end{cases} \tag{30}$$

where $u_k = u\big|_{\Omega_k} \quad \forall k \in \{1,\ldots,M\}$. In particular, the continuity on the boundary is ensured by the finite element chosen and by its relative shape function. Then the global displacement field u depends on $2N$ scalar translational parameters:

$$(U_l,V_l,)_{l\in\{1,..,N\}} . \tag{31}$$

These $2N$ independent parameters can be collected in the single vector:

$$\hat{U} = (U_1,V_1,..,U_j,V_j,..,U_N,V_N), \quad \hat{U} \in R^{2N}. \tag{32}$$

- The potential energy $\wp$, which is the potential energy of the external forces only, can be expressed again in terms of the components of $\hat{U}$, $\wp$ being the negative of the scalar product of the applied forces times the displacements of their points of application, that is a linear function of $2N$ unknown Lagrangian parameters, that can be symbolically expressed as follows:

$$\wp = \wp(\hat{U}) , \hat{U} \in R^{2N} . \tag{33}$$

The problem can be formulated, also in this case, as a linear programming one, in the form:

$$\min_{U\in K^N} \wp(\hat{U}) , \tag{34}$$

K^N being the subset of R^{2N} defined by the unilateral constraints approximating the convex cone Sym^+, and to which the latent strain E must belong. It remains to define explicitly the subset $K^N \subseteq R^{2N}$.

- The subset K^N of R^{2N} is identified by a number of inequalities on the latent strain E. In what follows we summarise how to write explicitly such unilateral restrictions in terms of the displacements of the nodes of each element Ω_k. Recalling that the displacement field in any finite element Ω_k can be expressed as follows:

$$u_k = u\big|_{\Omega_k} = \sum_{l=1}^{9} N_l^f(x,y)\cdot(U_l, V_l) \ , \tag{35}$$

the latent strain, obtained as the symmetric part of the gradient of u_k, is:

$$E_k = E\big|_{\Omega_k} = Sym\nabla u_k . \tag{36}$$

The latent strain has to belong to the semidefinite positive space Sym^+. This condition, in the 3d space $(\varepsilon_{11}, \varepsilon_{22}, \sqrt{2}\varepsilon_{12})$, is represented geometrically in Figure 3 where the intersection between the cone $C : detE \geq 0$ and the half-space $trE \geq 0$ is depicted.

Figure 3 Three-dimensional representation, in the space $(\varepsilon_{11}, \varepsilon_{22}, \sqrt{2}\varepsilon_{12})$, of the cone $C : detE \geq 0$ and of the plane $\pi : trE = 0$. The vector v is orthogonal to the π plane and points toward the half-space $trE \geq 0$. The intersection between the half-space and the cone is the semidefinite positive convex cone Sym^+. A generic vector E belonging to Sym^+ is represented (see online version for colours)

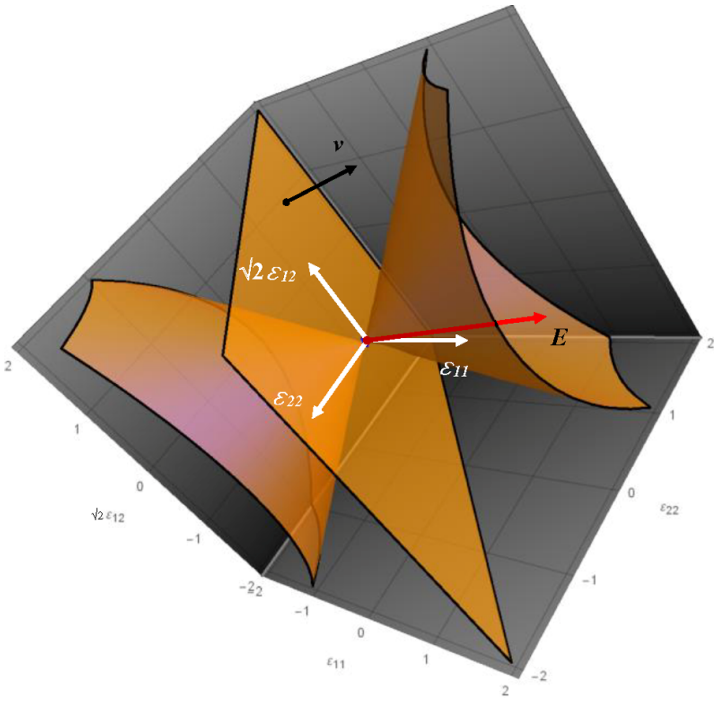

As already said, the condition on E is non-linear. Anyhow it is possible to approximate it with a finite set of linear relations, in order to reduce the non-linear problem to a linear one. This is done by linearly approximating the convex cone through a certain number p of tangent planes. The construction can be based on a set of points, equally spaced along a cross-section of the cone. At each point of this set we define a tangent plane. The set of all tangent planes constitutes an envelope of the cone. Increasing the number of points along the cross section the envelope produces a better fit of the conical surface Sym^+ as depicted in Figure 4.

Figure 4 In (a) envelope formed by 6 tangent planes and in (b) by 16 planes. The cross-section between the cone and a plane, orthogonal to the axis of the cone, is represented by the circumference on which a certain number of points are selected in order to 'generate' the plane envelope (see online version for colours)

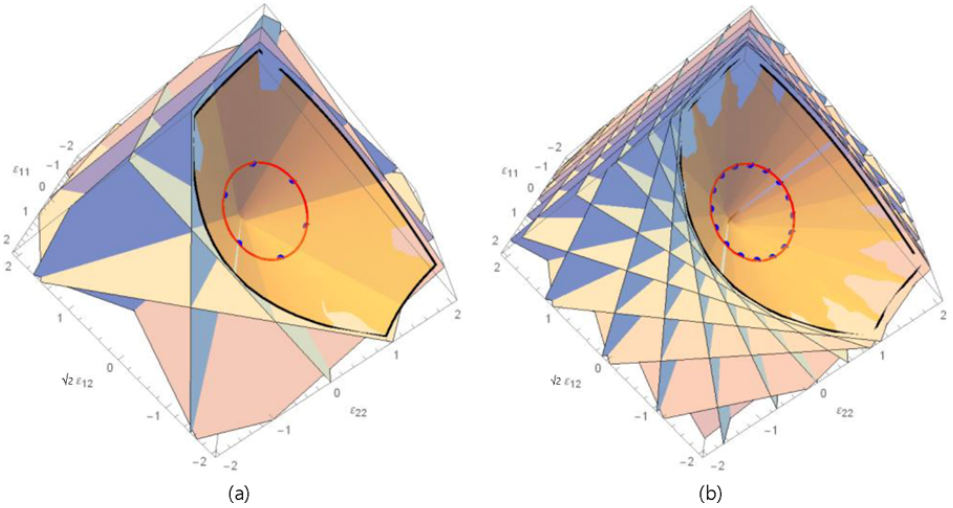

Thus, denoting $(\tilde{x},\tilde{y})$ the coordinates of a generic Gauss point of Ω_k, the non linear condition $E \in Sym^+$, can be written as:

$$E_k(\tilde{x},\tilde{y}) \in Sym^+ , \tag{37}$$

and in the approximate form (obtained using p tangent planes), transformed into the following set of inequalities:

$$A_k(\tilde{x},\tilde{y})\hat{U}_k \geq 0 , \tag{38}$$

where $A_k(\tilde{x},\tilde{y})$ is a matrix of p rows and $\hat{U}_k$ is the vector of the nodal displacements the element k.

The linearised condition $E \in Sym^+$ is then transformed into p linear inequalities that we enforce at 9 points, namely in the Gauss points of the element Ω_k, see Figure 5.

Figure 5 Envelope of the cone with 6 tangent planes and surface gradient vectors at the generating points. The condition $E_k(\tilde{x},\tilde{y}) \in Sym^+$ is discretised by using these gradient vectors to construct the system of inequalities $A_k(\tilde{x},\tilde{y})\hat{U}_k \geq 0$ (see online version for colours)

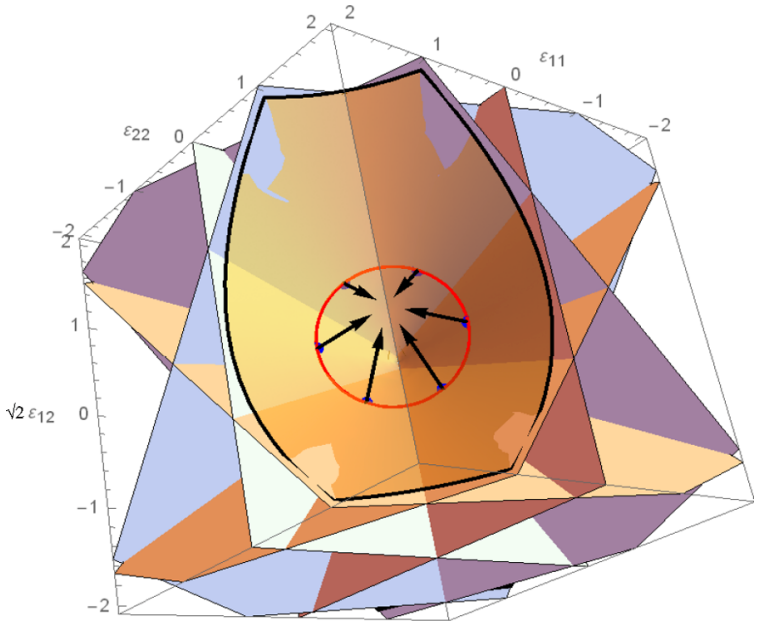

Collecting all these relations, for all elements, we have a set of unilateral constraints, of the type:

$$A\hat{U} \geq 0 \,. \tag{39}$$

These inequalities together with the boundary conditions restrict the vector $\hat{U} = (U_k, V_k)_{k\in\{1,..,N\}} \in R^{2N}$ to belong to the convex set

$$K^N = \{\hat{U} \in R^{2N} \,/\, A\hat{U} \geq 0\} \,. \tag{40}$$

- With the above approximation the structural problem is reduced to the following minimum problem: "*find a piecewise rigid displacement* $\hat{U}^0$ *which minimises the potential energy* $\wp$ *in* K^N *:*

$$\wp(\hat{U}^0) = \min_{U\in K^N} \wp(\hat{U}) \,." \tag{41}$$

This linear programming problem can be solved with a method of linear programming.

For a small number of variables it can be solved exactly with the simplex method (see Dantzig et al., 1955), and for large problems there exist a number of well-known, and efficient, approximate alternatives (see Mehrotra, 1992; Vanderbei, 2014; Dantzig, 1963).

- Once the minimiser $\hat{U}^0$ has been obtained it is an easy task to construct the deformed shape of the structure, and graphically represent the corresponding rotation and strain fields.

Remark 4: We have to point out that the appearance of piece-wise rigid mechanisms (producing concentrated fractures) rather than continuous mechanisms (entailing diffuse fractures), is often due, in real structures, to mechanical characteristics, such as cohesion, toughness and finite friction, which are not accounted for by the NRNT model.

Indeed for ideal NRNT materials, on an energetical ground, it is in general not possible to prefer one way of deformation over the other. This peculiar behaviour is essentially due to the absence of any growth property of the energy with respect to unbounded fracture strains. A growth property of the energy for displacement fields in $BD(\Omega)$ is restored by introducing the so-called "*Safe Load Condition*", a condition which is necessary, with the known theorems, to prove the existence of a displacement solution for the parent equilibrium problem concerning NENT materials, see Giaquinta and Giusti (1985) and Anzellotti (1985).

Indeed there is a legitimate way to encourage rigid block mechanisms over diffuse deformations. It consists in adding, all over the loaded boundary, a given uniform pressure of very small magnitude (say of the order of a magnitude of a small fraction of the atmospheric pressure). This trick is sufficient to provide the BVP with the "*Safe Load Condition*", and to make, in most of the examples, concentrated fractures (and then rigid block deformations) as the favourite minimising mechanisms. ■

5 Example 1: identification of a diagonal crack

Let us consider the case of a panel of NRNT material, loaded by its own weight and constrained as shown in Figure 6(a). This is a so called *mixed problem*, since part of the boundary is loaded and the remaining part is constrained. A portion of the bottom constraint is subjected to a given linear settlement as shown in Figure 6(a). A diagonal crack is expected, as a solution of the BVP, as shown with the slanted bold line in Figure 6(b).

Figure 6 Mixed BVP for a panel of NRNT material (loaded by its own weight and constrained as shown) subjected to a given linear settlement (a). A diagonal crack is expected (b) (see online version for colours)

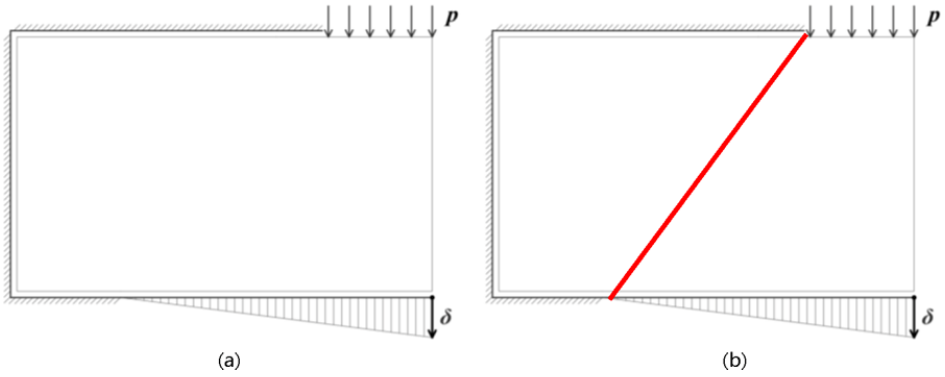

5.1 Example 1: analytical solution

Using singular strain and stress fields, a possible analytical solution of the mixed BVP (shown in Figure 6(a)) is represented in Figure 7.

Figure 7 A possible analytical solution of the BVP depicted in Figure 6(a), using a regular stress field T^r and a singular strain field E^s such that $T^r \cdot E^s = 0$, is reported. A hinge forms and the crosshatch in red represents the singular deformations E^s along the fracture line (see online version for colours)

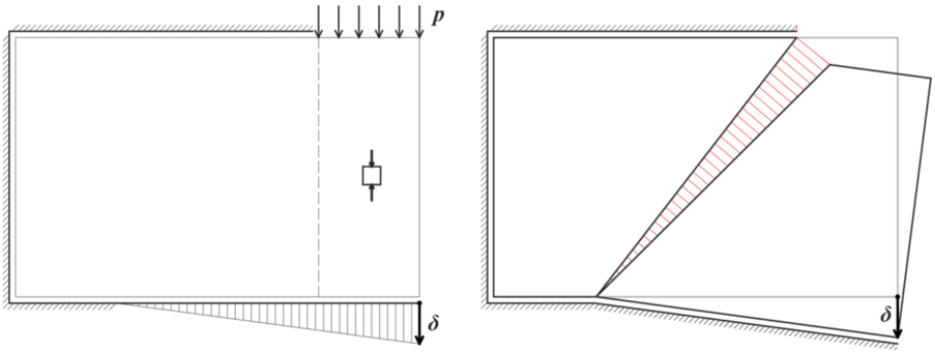

5.2 Example 1: C° method (square FE mesh)

The NRNT panel under the BVP described in Figure 6(a) is discretised into 240 square 9-node Lagrangian elements (Figure 8). We consider again a uniform load applied along the top (loaded) part of the boundary.

Figure 8 Panel of NRNT material discretised into 240 square 9-node finite elements. A portion of the constrained boundary is subjected to a given linear settlement as shown (see online version for colours)

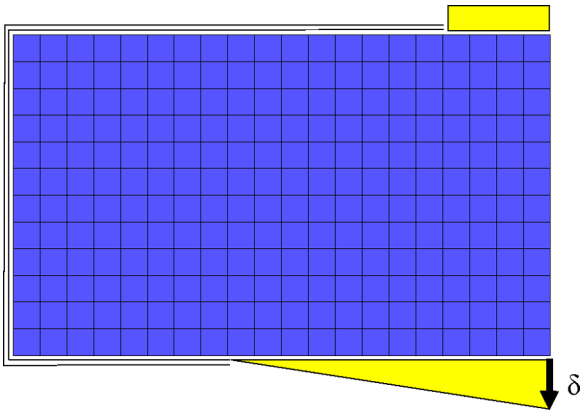

The solution $\hat{U}^0$ of this minimum problem is obtained through the interior point method in 600s (with an Intel® Core™ i7-6700HQ). The corresponding displacement is depicted in Figure 9.

Figure 9 Displacement field corresponding to the solution $\hat{U}^0$ of the problem (see online version for colours)

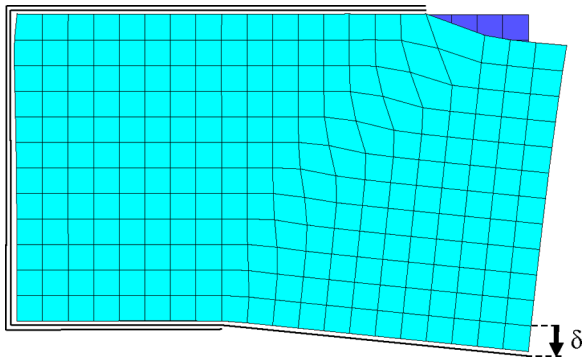

The streamlines of the displacement field reported in Figure 10(a) identify the point {2.0, 0.0} as possible centre of rotation. In Figure 10(b) to represent the strain field E, we report the graph of a measure of the deformation, namely the contour plot of $|E|^2 = tr(EE^T)$. From Figure 10(b), we see that the gradient of deformation is concentrated along a narrow band located in the vicinity of slanted line, whilst the other elements are characterised by strains whose norm is close to zero. The skew-symmetric part of the displacement field, representing the local rotation field, is depicted in Figure 10(c). It should be noticed that the gradient of rotation is also essentially concentrated along a diagonal line (Figure 10). By depicting the positive rotations in light grey (piers) and the negative ones in dark grey (Figure 10(d)), also in this case we obtain a neat subdivision of the domain into two blocks deforming as rigid bodies and a clear identification of the possible interface.

6 Example 3: a simple portal under horizontal load

In this section, we present two applications concerning a simple portal under horizontal actions analysed by using the C° method varying the modelling of the horizontal load. In order to solve the problem of a structure under horizontal action and then to evaluate the horizontal collapse multiplier λ_c, we proceed as follows: denoting with λ the scale factor of the horizontal actions (loads or displacements), we can find an interval $[\lambda_s, \lambda_m]$ to which the collapse multiplier λ_c has to belong. In particular, λ_s represents an approximation of the supremum of the multipliers for which the initial configuration is still safe (i.e., $\hat{U}^0 = 0$), whilst λ_m represents an approximation of the infimum of the multipliers for which the structure becomes a mechanism (i.e., $\hat{U}^0 \neq 0$).

6.1 Case A: distributed horizontal load

The NRNT portal, discretised with 384 9-nodes square elements (a second order Lagrangian quadrangular element), is loaded on the top edge by a piecewise uniformly distributed load q as shown in Figure 11(a). The external horizontal action is represented

by the horizontal distribution of loads (represented by strips with arrows) proportional to the vertical ones through the scale factor λ as shown in Figure 11(a).

Figure 10 Stream plot of the displacement field (a); field $|E|^2 = tr(EE^T)$ (b) and rotation field (c) over the whole domain. By depicting the positive and negative rotations with two different shades of grey, in (d) a neat partition of the whole domain into two rigid blocks is identified. The interface among the two blocks is in close agreement with the location of the expected crack (see online version for colours)

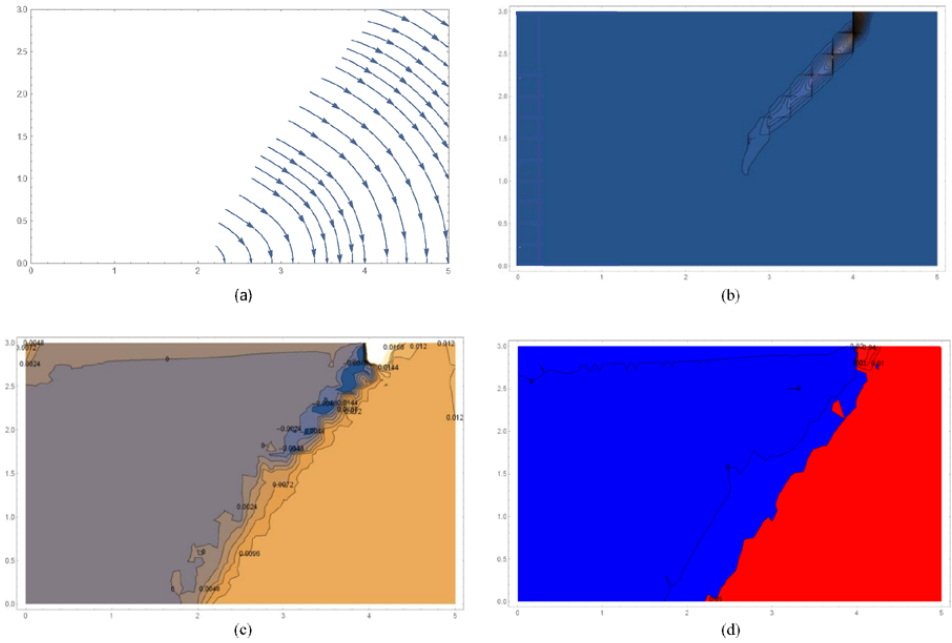

Figure 11 In (a) the NRNT portal, discretised with 384 9-nodes square elements, is loaded by a piecewise uniformly distributed vertical load and by a similar horizontal load distribution $0.255q$ (represented with the strips with horizontal arrows). In (b) a representation of the solution is depicted (see online version for colours)

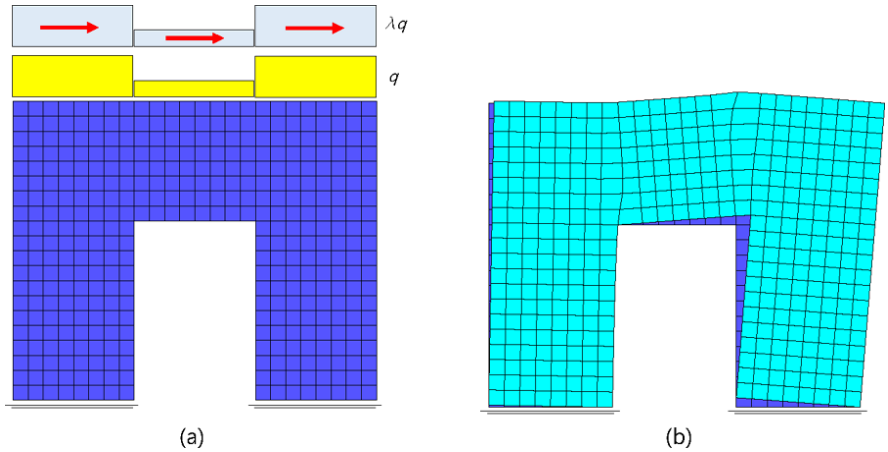

The collapse multiplier λ_c belongs to the interval $[0.252, 0.253]$ and this range is confirmed by applying directly the kinematical theorem on the detected mechanism. The solution $\hat{U}^0$ of the minimum problem, corresponding to $\lambda_m = 0.0253$, obtained with the interior point method in 716.78s (with an Intel® Core™ i7-6700HQ) by using 16 tangent planes for each node, is shown graphically in Figure 11(b). The streamlines of the displacement field are reported in Figure 12.

Figure 12 The stream plot of the displacement field is reported: the centres of rotation can be identified (see online version for colours)

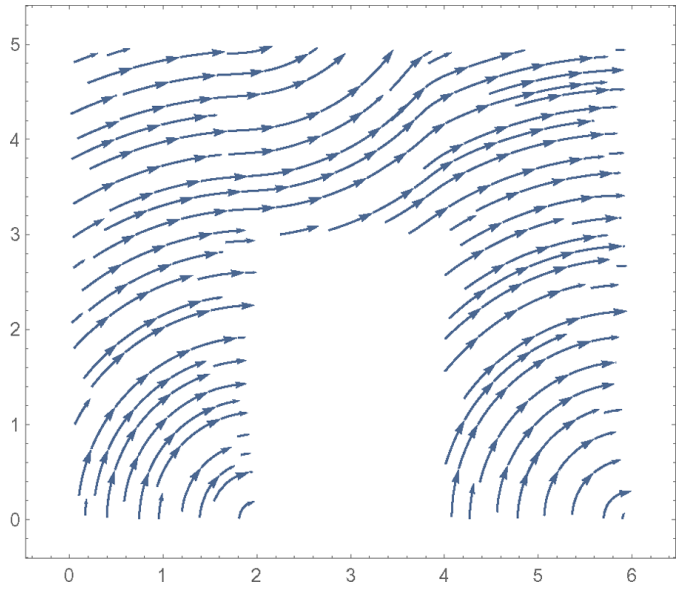

To represent the strain field E, in Figure 13 we report a measure of the deformation, namely $|E|^2 = tr\left(EE^T\right)$.

The skew-symmetric part of the displacement field is depicted Figure 14(a). It should be noticed that the gradient of rotation is essentially concentrated along two vertical lines. By depicting the positive rotations in light grey and the negative ones in dark grey (Figure 14(b)) we obtain a neat subdivision of the domain into three blocks. Such blocks deform essentially as rigid bodies since the rotation is piece-wise constant and the deformation is practically constant (see Figure 13).

6.2 Case B: concentrated horizontal load

The same NRNT portal of Figure 11(a) is still discretised using 384 9-nodes square, and also in this case the vertical load is applied on the top edge trough a piecewise uniformly distributed load q as shown in Figure 15(a). The external horizontal action is here represented by the force λQ where Q is equal to the resultant of the acting vertical loads and λ is the scale factor.

Figure 13 The field $|E|^2 = tr(EE^T)$ is reported (see online version for colours)

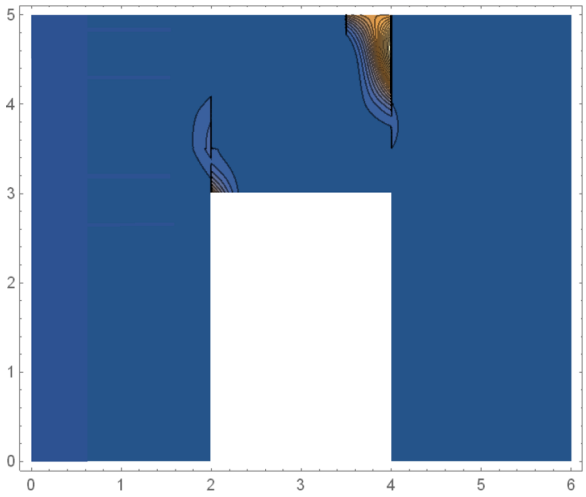

Figure 14 In (a) the rotation field over the whole domain. In (b) by depicting the positive rotations in light grey and the negative ones in dark grey, a neat partition of the whole domain into three rigid blocks can be seen (see online version for colours)

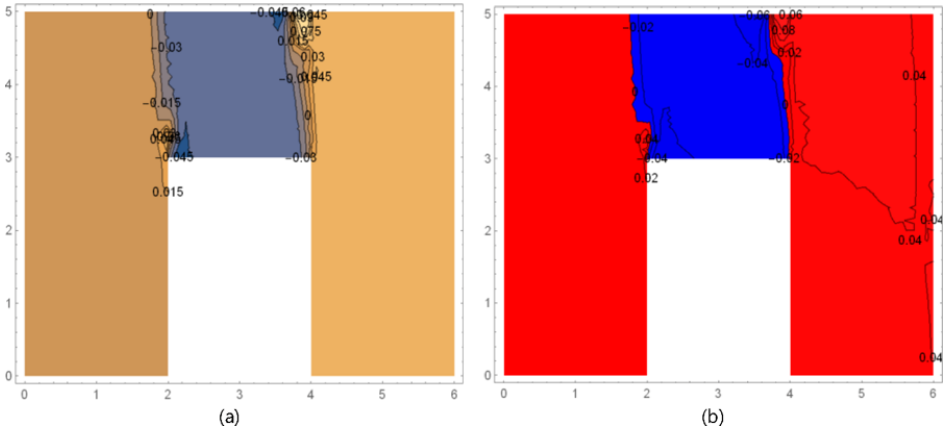

The collapse multiplier λ_c belongs to the interval $[0.31, 0.32]$ as can be checked applying directly the upper bound theorem on the detected failure mechanism. As in the previous case, these last values are supported by the direct analysis of the kinematical theorem on the identified mechanism of failure. The solution $\hat{U}^0$ of the minimum problem, obtained with the interior point method in 628.54s (with an Intel® Core™ i7-6700HQ) by using 16 tangent planes for each node, is shown graphically in Figure 15(b). The streamlines of the displacement field are reported in Figure 16.

To represent the strain field E, in Figure 17 we report a measure of the deformation, namely $|E|^2 = tr(EE^T)$.

Figure 15 In (a) the NRNT portal, discretised with 384 9-nodes square elements, is loaded by a piecewise uniformly distributed vertical load and by a similar horizontal force λQ. In (b) a representation of the solution corresponding to $\lambda = 0.32$ is depicted (see online version for colours)

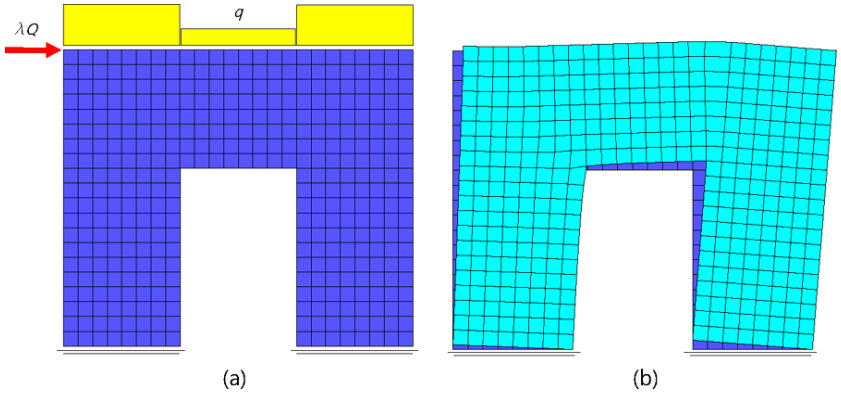

Figure 16 Stream plot of the displacement field: the rotation centres are easily identified (see online version for colours)

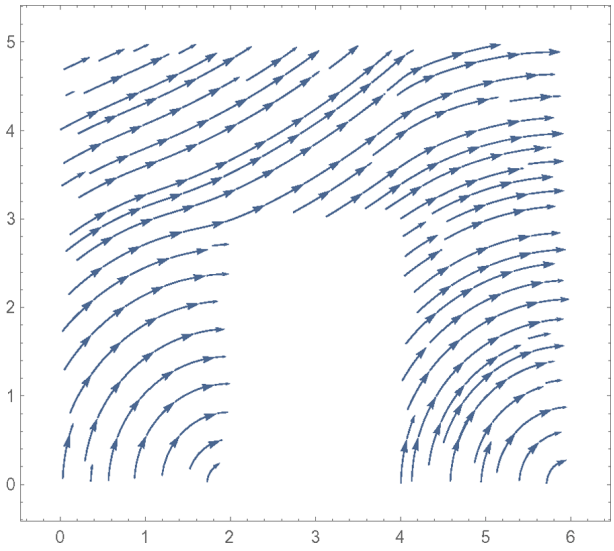

The skew-symmetric part of the displacement field is depicted in Figure 18. It should be noticed that the gradient of rotation is essentially concentrated along two lines. By depicting the positive rotations in light grey and the negative ones in dark grey (Figure 18(b)), we obtain a neat subdivision of the domain into three blocks. As in the previous case, such blocks deform essentially as rigid bodies since the rotation is piece-wise constant and the deformation is almost everywhere constant (see Figure 17).

Figure 17 Representation of the field $|E|^2 = tr(EE^T)$ (see online version for colours)

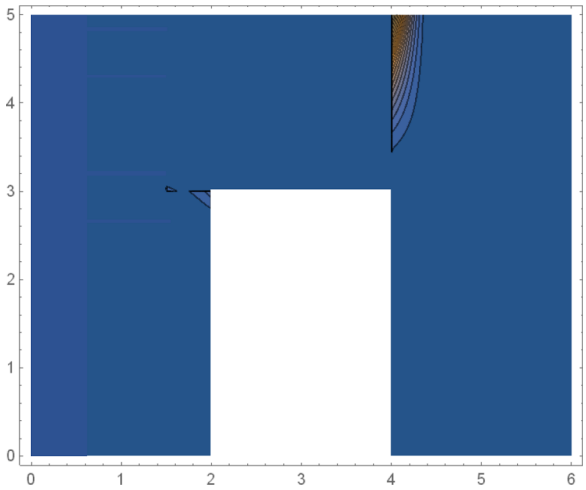

Figure 18 In (a) the rotation field over the whole domain. In (b) by depicting the positive rotations in light grey and the negative ones in dark grey, a neat partition of the whole domain into three rigid blocks can be seen (see online version for colours)

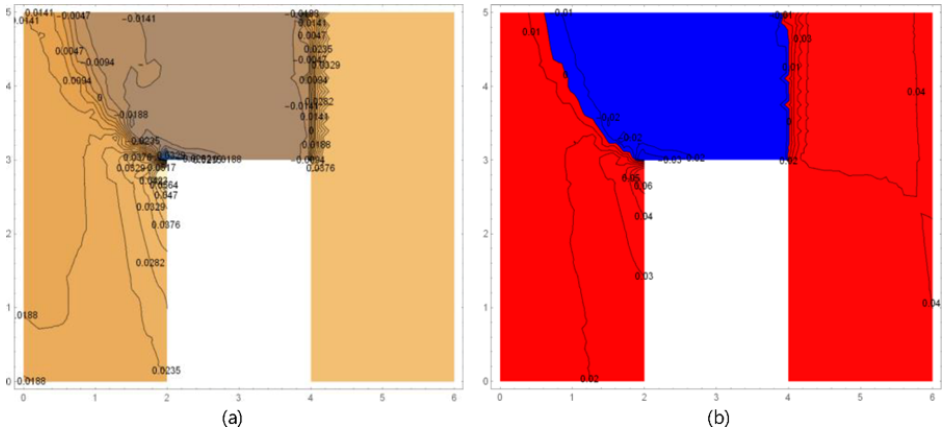

7 Example 4: a double portal under horizontal action

In this section, we present a different application of the C° method: a double portal subjected to a horizontal action modelled as horizontal linear displacement.

A NRNT double portal, discretised using 768 *9-nodes* square elements (a second order Lagrangian quadrangular element), is loaded vertically by two piecewise uniformly distributed loads, whilst the horizontal action is modelled by a linear displacement imposed to the left side of the structure as shown in Figure 19(a).

Figure 19 In (a) the NRNT double portal, discretised with 768 9-nodes square elements, is loaded by a piecewise uniformly distributed load and is subjected at left side to a linear distribution of displacements. In (b) a representation of the solution is depicted (see online version for colours)

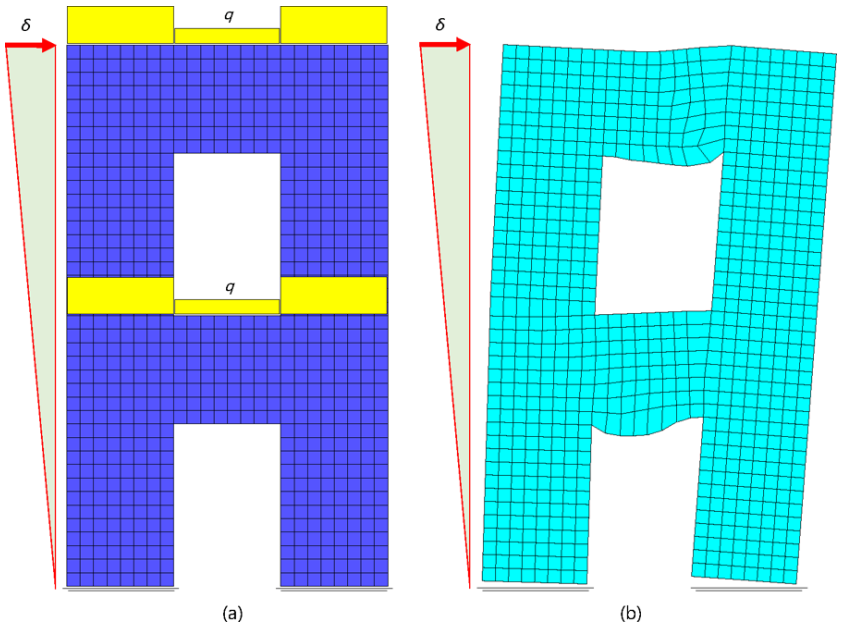

The solution $\hat{U}^0$ of the minimum problem is reached through the minimisation of the energy into the finite element space defined previously (see Section 3). The solution obtained with the interior point method in 600s (with an Intel® Core™ i7-6700HQ) is shown graphically in Figure 19(b). The horizontal component of the displacement corresponding to the solution $\hat{U}^0$ is reported in Figure 20: the gradient of the displacement field is concentrated essentially along lines.

Figure 20 Graph of the horizontal component of the displacement field corresponding to the solution $\hat{U}^0$ (see online version for colours)

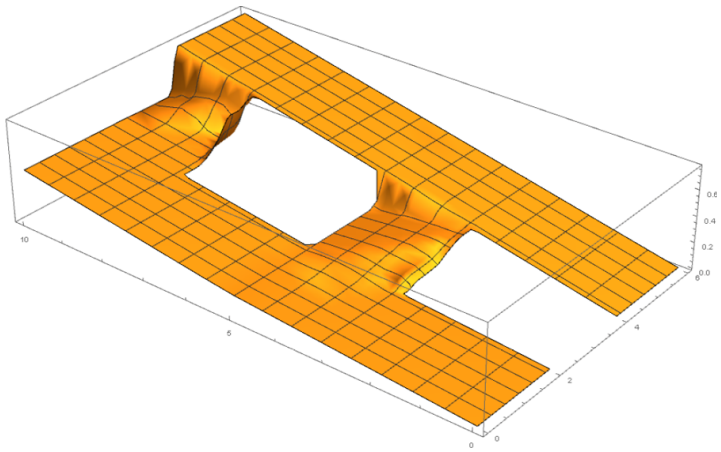

The skew-symmetric part of the displacement field (representing the local rotation) is depicted in Figure 21(a). It should be noticed that the gradient of rotation is essentially concentrated along lines (Figure 21(a)). From the stream plot of the displacement field over the whole domain (Figure 21(b)) the centres of rotation can be clearly identified. By depicting the positive rotations in light grey and the negative ones in dark grey (Figure 22(a)), we obtain a neat subdivision of the domain into five blocks Figure 22(b). Such blocks deform essentially as rigid bodies since the rotation and the deformation are piecewise constant. Notice that the strain, though we are using continuous functions, is practically all concentrated on lines.

Figure 21 Rotation field over the whole domain: (a). Stream plot of the displacement field: (b) (see online version for colours)

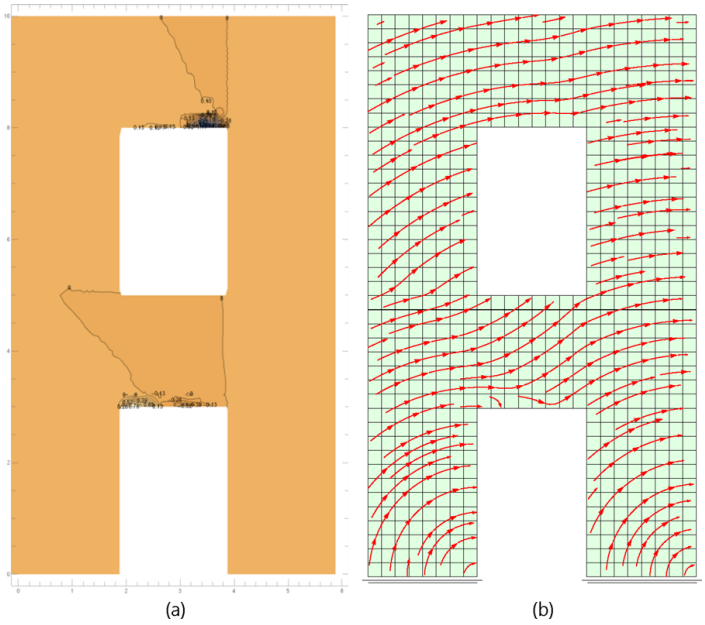

8 Example 5: validation of the C° method with an experimental test

This final example concerns a full-scale masonry wall subjected to fixed vertical loads on the piers and to an in-plane, gradually increasing, horizontal force as sketched in Figure 23(a). The panel has been experimentally tested by Augenti et al. as reported in Augenti et al. (2010). A comparison of the results of the proposed model with the experimental ones is carried out providing a validation of the proposed approach. For brevity, we omit the details of the experiments, making reference directly to Augenti et al. (2010). In particular the values of the given vertical loads, the way such loads are transmitted to the panel, and the constraint conditions considered at the base of the piers, resemble closely those adopted in the test.

The solution $\hat{U}^0$ of the minimum problem obtained with our numerical method is represented pictorially in Figure 23(b) together with the value of the load producing the activation of the mechanism (180 kN).

Figure 22 By depicting the positive rotations in light grey and the negative ones in dark grey (a), a neat partition of the whole domain into five rigid blocks can be seen (b) (see online version for colours)

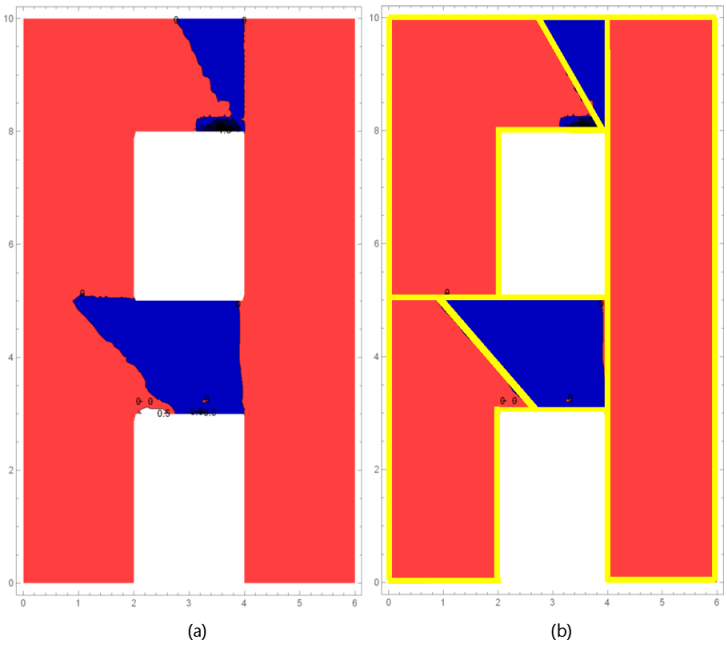

Figure 23 Masonry panel (experimentally tested, see Augenti et al. (2010): geometry, vertical and horizontal loads and discretisation (a); representation of the solution $\hat{U}^0$ in terms of displacements (b) (see online version for colours)

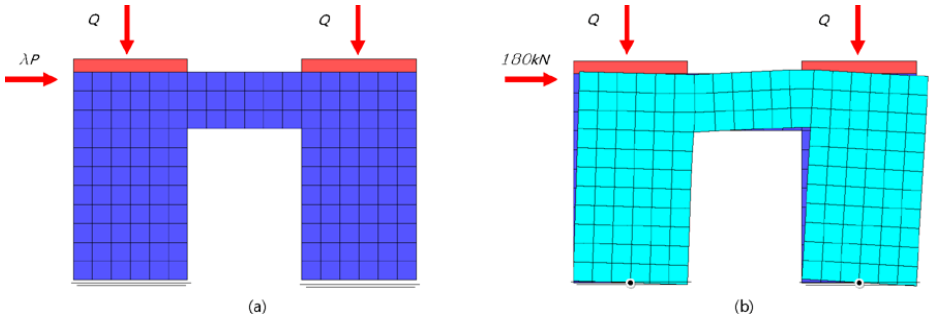

Figure 24 shows the post-processing of the solution. More specifically, Figure 24(a) depicts the contour plot of $|E|^2 = tr\left(EE^T\right)$, Figure 24(b) represents the stream plot of the displacement field, Figure 24(c) plots the rotation field whose signs are reported in Figure 24(d). From these figures we see that the C° model allows to detect in clear manner the rigid blocks and the strain concentration, the collapse mechanism of the structure under horizontal actions and a clear localisation of cracks

Figure 24 Post-processing of the solution: representation of the field $|E|^2 = tr(EE^T)$ (a), stream plot of the displacement field (b), sketch of the rotation field (c), signs of the rotations: light grey (piers) clockwise and dark grey (spandrel) counter-clockwise (d) (see online version for colours)

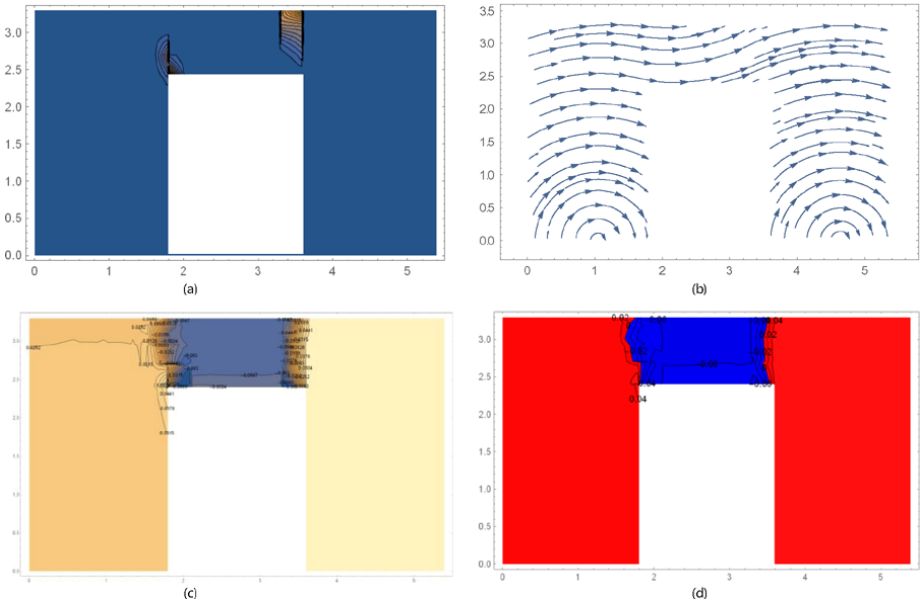

Figure 25(a) shows the mechanism of the structure involving rotations of the piers and of the spandrel. In particular, the shape of the cracks and the position of the centres of relative rotation suggested by the C° solution, indicate that the spandrel behaves as a compressed strut. The corresponding crack pattern resembles closely the one depicted in Figure 25(b) that reports the damages observed in the experimental test described in Augenti et al. (2010).

Figure 25 Mechanism predicted by the proposed C° method (a); the rotations of the piers and spandrel are consistent with those reported in Figure 24(a), d. Crack pattern observed in the experimental test reported by Augenti et al. (2010) (see online version for colours)

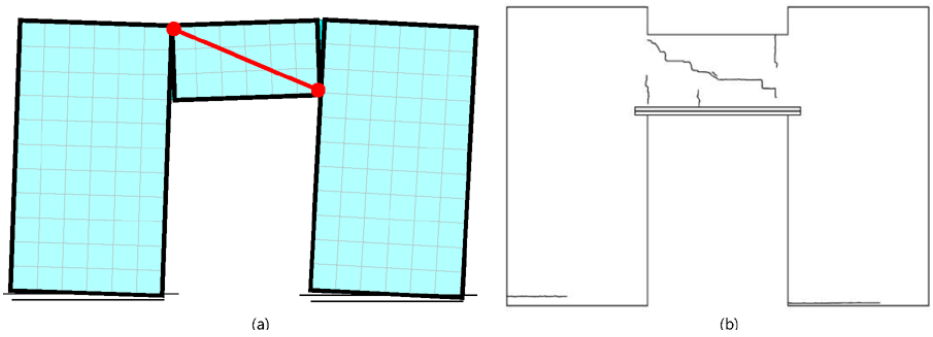

In Figure 25(b), a diagonal crack, tracing essentially the boundaries of the diagonal compressed strut depicted in Figure 25(a), can be identified. Such cracks are produced by small sliding/crushing deformations that develop into the spandrel at high levels of load.

Such cracks, that cannot be predicted by our model for which the material is infinitely resistant in compression, have scant effect on the overall mechanism of the structure and on the associated 'collapse' load. More experimental comparisons can be analysed adopting the experimental evidences by Beyer and Dazio (2012) and Gattesco et al. (2008).

9 Conclusions

A computer program detecting the fracture patterns due to a set of settlements/distortions applied on a loaded masonry-like structures has been developed and tested. By following Heyman hypotheses, masonry is considered as a continuous medium composed of unilateral material, perfectly rigid in shortening and perfectly soft in elongation, satisfying a normality law, i.e., Normal Rigid No-Tension (NRNT) material. The material is rigid in compression, but extensional deformations (fracture), allowed at zero energy price, can be either regular or singular; then extensional deformation can appear either as concentrated (macroscopic cracks) or diffuse (smeared cracks). The fact that rigid block deformation seems to be the preferred failure mode for real masonry structures stems from mechanical characteristics, such as toughness, interlocking, finite friction and cohesion, which are not inherent to the NRNT model. The equilibrium problem has been solved as an energy minimum operating numerically in the set of continuous C° displacement fields, by adopting for the geometrical description a classical Finite Element approximation and detecting the crack as a system of smeared cracks.

In real masonry structures, the main question of a fracture investigation is a problem of identification, that is consists in identifying the system of settlements and distortions on the construction that produced the detected crack pattern. The computer code we have developed here, being a deterministic tool able to find the mechanism and the fracture pattern due to known kinematical data, can represent an essential device of any specific structural identification code. Actually, there are many studies proposing macro-block analyses (see for example Sarhosis et al. (2016) and references therein) and there exists an extensive literature on the so-called *discrete element approximation* of real masonry structures (the recent book (Drei et al., 2016) may be consulted for reference). The present study represents an efficient alternative to more sophisticated numerical models (as, described, for example in Milani et al. (2012), Bertolesi et al. (2016), Chiozzi et al. (2017) and Addessi and Sacco (2016, 2018)), not requiring any guess concerning the partition into macro-blocks, such a partition being actually a result of the analysis.

Indeed, in the examples that we present, the subdivision into macroblocks can arises naturally in solving the minimisation problem. The subdivisions into macro-blocks predicted by our analysis in a number of simple examples, is in good agreement with the ones which are expected either through analytical solutions or experiments. We must say that C° method is more cumbersome numerically with respect to other approximation methods, due both to the larger number of constraints and to the finer meshes required for the approximation of the large displacement gradients which are necessary to approximate macroscopic fractures. With the C° method, the subdivision into blocks must be, sometimes, encouraged by applying a fictitious uniform pressure on the whole loaded boundary. This pressure, which prevents unbounded elongations at zero energy cost, is usually a negligible fraction of the applied loads (two orders of magnitude less than the atmospheric pressure).

The orientation of the cracks is accurately detected by considering approximate solutions based on the C° method, as shown in the reported examples. In particular, an application involving a masonry panel experimentally tested has been reported. The comparison of the experimental outcomes with the analytical ones confirms the validity of the proposed model.

References

Addessi, D. and Sacco, E. (2016) 'Nonlinear analysis of masonry panels using a kinematic enriched plane state formulation', *International Journal of Solids and Structures*, Vol. 90, pp.194–214.

Addessi, D. and Sacco, E. (2018) 'Homogenization of heterogeneous masonry beams', *Meccanica*, Vol. 53, No. 7, pp. 1699–1717.

Angelillo, M. (2014) 'Practical applications of unilateral models to masonry equilibrium', in Angelillo, M. (Ed.): *Mechanics of Masonry Structures*, Vienna, Springer, pp.109–210.

Angelillo, M. (2015) 'Static analysis of a guastavino helical stair as a layered masonry shell', *Composite Structures*, Vol. 119, pp.298–304.

Angelillo, M. and Fortunato, A. (2004) 'Equilibrium of masonry vaults', in Fremond, M. and Maceri, F. (Eds.): *Lecture Notes in Applied and Computational Mechanics, Novel Approaches in Civil Engineering,* Vol. 14, pp.105–111.

Angelillo, M., Babilio, E. and Fortunato, A. (2005) 'A numerical method for fracture of rods', in Fremond, M. and Maceri, F. (Eds.): *Lecture Notes in Applied and Computational Mechanics, Mechanical Modelling and Computational Issues in Civil Engineering*, Vol. 23, pp.277–292.

Angelillo, M., Babilio, E. and Fortunato, A. (2012) 'Numerical solutions for crack growth based on the variational theory of fracture', *Computational Mechanics*, Vol. 50, No. 3, pp.285–301.

Angelillo, M., Babilio, E., Fortunato, A., Lippiello, M. and Montanino, A. (2016) 'Analytic solutions for the stress field in static sandpiles', *Mechanics of Materials*, Vol. 95, pp.192–203.

Angelillo, M., Cardamone, L. and Fortunato, A. (2010) 'A numerical model for masonry-like structures', *Journal of Mechanics of Materials and Structures*, Vol. 5, No. 4, pp.583–615.

Angelillo, M., Fortunato, A., Montanino, A. and Lippiello, M. (2014) 'Singular stress fields in masonry structures: derand was right', *Meccanica*, Vol. 49, No. 5, pp.1243–1262.

Anzellotti, G. (1985) 'A class of convex non-coercive functionals and masonry-like materials', *Annales De l'IHP Analyse Non Linéaire*, Vol. 2, No. 4, pp.261–307.

Augenti, N., Parisi, F., Prota, A. and Manfredi, G. (2010) 'In-plane lateral response of a full-scale masonry subassemblage with and without an inorganic matrix-grid strengthening system', *Journal of Composites for Construction*, Vol. 15, No. 4, pp.578–590.

Bathe, K.J. and Wilson, E.L. (1976) *Numerical Methods in Finite Element Analysis*, Prentice-Hall, Englewood Cliffs, New Jersey, USA.

Bertolesi, E., Milani, G. and Lourenço, P.B. (2016) 'Implementation and validation of a total displacement non-linear homogenization approach for in-plane loaded masonry', *Computers and Structures*, Vol. 176, pp.13–33.

Beyer, K. and Dazio, A. (2012) 'Quasi-static cyclic tests on masonry spandrels', *Earthquake Spectra*, Vol. 28, No. 3, pp.907–929.

Brandonisio, G., Lucibello, G., Mele, E. and De Luca, A. (2013) 'Damage and performance evaluation of masonry churches in the 2009 L'Aquila earthquake', *Engineering Failure Analysis*, Vol. 34, pp.693–714.

Brandonisio, G., Mele, E. and De Luca, A. (2015) 'Closed form solution for predicting the horizontal capacity of masonry portal frames through limit analysis and comparison with experimental test results', *Engineering Failure Analysis*, Vol. 55, pp.246–270.

Calderoni, B., Prota, A., Cordasco, E.A. and Sandoli, A. (2016) 'Seismic vulnerability of ancient'masonry buildings and strengthening intervention strategies', *Proceedings of XVI IBMAC International Conference*, pp.727–736.

Cennamo, C. and Di Fiore, M. (2013) 'Structural, seismic and geotechnical analysis of the sant'Agostino church in L'aquila', *Revista Ingeniería De Construcción*, Vol. 28, No. 1, pp.7–20.

Cennamo, C., Angelillo, M. and Cusano, C. (2017) 'Structural failures due to anthropogenic sinkholes in the urban area of naples and the effect of a FRP retrofitting', *Composites Part B: Engineering*, Vol. 108, pp.190–199.

Cennamo, C., Gesualdo, A. and Monaco, M. (2017) 'Shear plastic constitutive behaviour for near-fault ground motion', *Journal of Engineering Mechanics ASCE*, Vol. 143, No. 9, p.04017086.

Chambolle, A., Giacomini, A. and Ponsiglione, M. (2007) 'Piecewise rigidity', *Journal of Functional Analysis*, Vol. 244, No. 1, pp.134–153.

Chiozzi, A., Milani, G. and Tralli, A. (2017) 'A genetic algorithm NURBS-based new approach for fast kinematic limit analysis of masonry vaults', *Computers and Structures*, Vol. 182, pp.187–204.

Como, M. (1992) 'On the equilibrium and collapse of masonry structures', *Meccanica*, Vol. 27, No. 3, pp.185–194.

Dantzig, G. (1963) *Linear Programming and Extensions*, Princeton University Press, Princeton, New Jersey, USA.

Dantzig, G.B., Orden, A. and Wolfe, P. (1955) 'The generalized simplex method for minimizing a linear form under linear inequality restraints', *Pacific Journal of Mathematics*, Vol. 5, No. 2, pp.183–195.

De Serio, F., Angelillo, M., De Chiara, E., Gesualdo, A., Iannuzzo, A., Zuccaro, G. and Pasquino, M. (2017) 'Masonry structures made of monolithic blocks with an application to spiral stairs', *Meccanica*, pp.1–21, doi: 10.1007/s11012-017-0808-9.

Drei, A., Milani, G. and Sincraian, G. (2016) 'Application of DEM to historic masonries, two case-studies in portugal and italy: aguas livres aqueduct and arch-Tympana of a church', *Computational Modeling of Masonry Structures Using the Discrete Element Method*, IGI Global, pp.326–366.

Fortunato, A., Babilio, E., Lippiello, M., Gesualdo, A. and Angelillo, M. (2016) 'Limit analysis for unilateral masonry-like structures', *The Open Construction and Building Technology Journal*, Vol. 10, Suppl 2: M12, pp.346–362.

Fortunato, A., De Chiara, E., Fraternali, F. and Angelillo, M. (2015) 'Advanced models for the limit analysis of masonry structures', *COMPDYN 2015*, *5th ECCOMAS Thematic Conference on Computational Methods in Structural Dynamics and Earthquake Engineering Crete Island COMPDYN 2015*, pp.3716–3725.

Fortunato, A., Fabbrocino, F., Angelillo, M. and Fraternali, F. (2018) 'Limit analysis of masonry structures with free discontinuities', *Meccanica*, Vol. 53, No. 7, pp.1793–1802.

Fortunato, A., Fraternali, F. and Angelillo, M. (2014) 'Structural capacity of masonry walls under horizontal loads', *Ingegneria Sismica*, Vol. 31, No. 1, pp.41–49.

Fraldi, M., Nunziante, L., Gesualdo, A. and Guarracino, F. (2009) 'On the bounding of limit multipliers for combined loading', *Proceedings of the Royal Society of London A: Mathematical, Physical and Engineering Sciences*, Vol. 466, No. 2114, pp.493–514.

Gattesco, N., Clemente, I., Macorini, L. and Noè, S. (2008) 'Experimental investigation on the behaviour of spandrels in ancient masonry buildings', *Proceedings of 14th WCEE*, 12–17 October, Beijing, China.

Gesualdo, A. and Monaco, M. (2015) 'Constitutive behaviour of quasi-brittle materials with anisotropic friction', *Latin American Journal of Solids and Structures*, Vol. 12, No. 4, pp.695–710.

Gesualdo, A., Cennamo, C., Fortunato, A., Frunzio, G., Monaco, M. and Angelillo, M. (2017) 'Equilibrium formulation of masonry helical stairs', *Meccanica*, Vol. 52, No. 8, pp.1963–1974.

Gesualdo, A., Iannuzzo, A., Monaco, M. and Penta, F. (2017) 'Rocking of a rigid block freestanding on a flat pedestal', *Journal of Zhejiang University: Science A*, pp.1–10, DOI: 10.1631/jzus. A1700061.

Gesualdo, A., Iannuzzo, A., Monaco, M. and Savino, M.T. (2014) 'Dynamic analysis of freestanding rigid blocks', *CIVIL-COMP PROCEEDINGS, Twelfth International Conference on Computational Structures Technology*, Paper 144.

Giaquinta, M. and Giusti, E. (1985) 'Researches on the equilibrium of masonry structures', *Archive for Rational Mechanics and Analysis*, Vol. 88, No. 4, pp.359–392.

Heyman, J. (1966) 'The stone skeleton', *International Journal of Solids and Structures*, Vol. 2, No. 2, pp.249–279.

Iannuzzo, A., Angelillo, M., De Chiara, E., De Guglielmo, F., De Serio, F., Ribera, F. and Gesualdo, A. (2018) 'Modelling the cracks produced by settlements in masonry structures', *Meccanica*, Vol. 53, No. 7, pp.1857–1873.

Kooharian, A. (1952) 'Limit analysis of voussoir (Segmental) 'and concrete archs', *Journal of the American Concrete Institute*, Vol. 24, No. 4, pp.317–328.

Livesley, R.K. (1978) 'Limit analysis of structures formed from rigid blocks', *International Journal for Numerical Methods in Engineering*, Vol. 12, No. 12, pp.1853–1871.

Marmo, F., Masi, D. and Rosati, L. (2018) 'Thrust network analysis of masonry helical staircases', *International Journal of Architectural Heritage*, DOI: 10.1080/15583058.2017.1419313.

Marmo, L. and Rosati, L. (2017) 'Reformulation and extension of the thrust network analysis', *Computers and Structures*, Vol. 182, pp.104–111.

Mehrotra, S. (1992) 'On the implementation of a primal-dual interior point method', *SIAM Journal on Optimization*, Vol. 2, No. 4, pp.575–601.

Milani, G. and Lourenço, P.B. (2012) '3D non-linear behavior of masonry arch bridges', *Computers and Structures*, Vol. 110, pp.133–150.

Monaco, M., Guadagnuolo, M. and Gesualdo, A. (2014) 'The role of friction in the seismic risk mitigation of freestanding art objects', *Natural Hazards*, Vol. 73, No. 2, pp.389–402.

Sarhosis, V., Bagi, K., Lemos, J.V. and Milani, G. (Eds.) (2016) *Computational Modelling of Masonry Structures Using the Discrete Element Method*, IGI Global.

Simon, J. and Bagi, K. (2016) 'Discrete element analysis of the minimum thickness of oval masonry domes', *International Journal of Architectural Heritage*, Vol. 10, No. 4, pp.457–475.

Vanderbei, R.J. (2014) *Linear Programming: Foundations and Extensions*, Springer-Verlag, New York, USA.

Wolfram, S. (2003) *The Mathematica Book*, 5th ed., Wolfram Media.